

International Journal of Modern Physics E  
© World Scientific Publishing Company

## $\bar{K}$ -NUCLEAR DEEPLY BOUND STATES? \*

AVRAHAM GAL

*Racah Institute of Physics, The Hebrew University  
Jerusalem 91904, Israel  
avragal@vms.huji.ac.il*

Received (15 May 2006)

Accepted (xx yy 2006)

Following the prediction by Akaishi and Yamazaki of relatively narrow  $\bar{K}$ -nuclear states, deeply bound by over 100 MeV where the main decay channel  $\bar{K}N \rightarrow \pi\Sigma$  is closed, several experimental signals in stopped  $K^-$  reactions on light nuclei have been interpreted recently as due to such states. In this talk I review (i) the evidence from  $K^-$ -atom data for a *deep*  $\bar{K}$ -nucleus potential, as attractive as  $V_{\bar{K}}(\rho_0) \sim -(150 - 200)$  MeV at nuclear matter density, that could support such states; and (ii) the theoretical arguments for a *shallow* potential,  $V_{\bar{K}}(\rho_0) \sim -(40 - 60)$  MeV. I then review a recent work by Mareš, Friedman and Gal in which  $\bar{K}$ -nuclear bound states are generated dynamically across the periodic table, using a RMF Lagrangian that couples the  $\bar{K}$  to the scalar and vector meson fields mediating the nuclear interactions. The reduced phase space available for  $\bar{K}$  absorption from these bound states is taken into account by adding a density- and energy-dependent imaginary term, underlying the corresponding  $\bar{K}$ -nuclear level widths, with a strength constrained by  $K^-$ -atom fits. Substantial polarization of the core nucleus is found for light nuclei, with central nuclear densities enhanced by almost a factor of two. The binding energies and widths calculated in this dynamical model differ appreciably from those calculated for a static nucleus. These calculations provide a lower limit of  $\Gamma_{\bar{K}} \sim 50 \pm 10$  MeV on the width of nuclear bound states for  $\bar{K}$  binding energy in the range  $B_{\bar{K}} = 100 - 200$  MeV.

### 1. Introduction

The  $\bar{K}$ -nucleus interaction near threshold is strongly attractive and absorptive as suggested by fits to the strong-interaction shifts and widths in  $K^-$ -atom levels<sup>1</sup>. Global fits yield ‘deep’ optical potentials  $V_{\bar{K}}(\rho_0) \sim -(150 - 200)$  MeV<sup>2,3,4,5</sup>, whereas other, more theoretically inclined works that fit the low-energy  $K^-p$  reaction data, including the  $I = 0$  unstable bound state  $\Lambda(1405)$  as input for constructing a density dependent optical potential, suggest relatively ‘shallow’ potentials with  $V_{\bar{K}}(\rho_0) \sim -(40 - 60)$  MeV<sup>6,7,8,9</sup>. The issue of the depth of the attractive  $\bar{K}$ -nucleus potential is briefly reviewed in Sections 2,3.

\*Dedicated to Walter Greiner on the occasion of his 70th birthday, presented at the International Symposium on Heavy Ion Physics, ISHIP 2006, Frankfurt, April 2006.

2 Avraham Gal

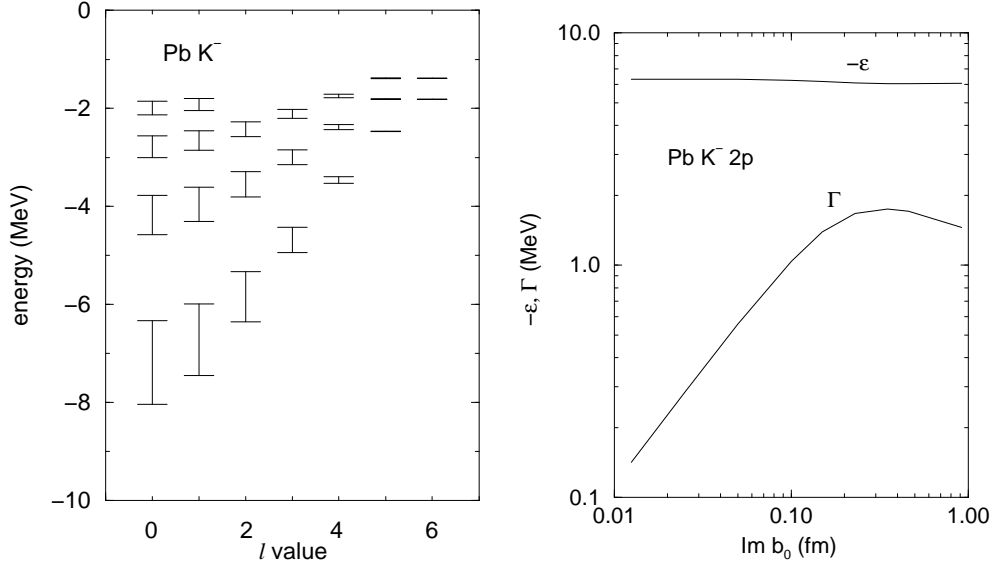


Fig. 1. Left: calculated spectrum of  $K^-$  ‘deeply bound’ atomic states in  $^{208}\text{Pb}$ . Right: saturation of width  $\Gamma$  for the  $2p$   $K^-$ - $^{208}\text{Pb}$  atomic state as function of  $\text{Im } b_0$ , for  $\text{Re } b_0 = 0.62$  fm.

It is instructive at this introductory stage to mention that irrespective of the depth of the real part of the potential, and quite paradoxically due to its strong imaginary (absorptive) part, relatively narrow  $K^-$  *deeply bound atomic states* were predicted to exist<sup>10,11</sup>, also confirmed in Ref. <sup>8</sup>. Figure 1 from Ref. <sup>11</sup> shows on the left-hand side a calculated spectrum of  $K^-$  atomic states in  $^{208}\text{Pb}$  where, in particular, all the circular states below the  $7i$  ( $l = 6$ ) state are not populated by X-ray transitions due to the strong  $K^-$ -nuclear absorption, and on the right-hand side it demonstrates saturation of the  $2p$  atomic-state width as a function of the absorptivity parameter  $\text{Im } b_0$  of the optical potential. The physics behind is that a strong imaginary part of  $V_{\bar{K}}$  acts repulsively, suppressing the *atomic* wavefunction in the region of overlap with  $\text{Im } V_{\bar{K}}$ . The calculated width of the ‘deeply bound’ atomic  $1s$  and  $2p$  is less than 2 MeV, calling for experimental ingenuity how to form these levels selectively by a non radiative process<sup>12</sup>. Relatively narrow  $\bar{p}$  deeply bound atomic states were also predicted, due to the same width saturation mechanism<sup>11</sup>.

This saturation mechanism does not hold for nuclear states which retain very good overlap with the potential. Hence, the question to ask is whether it is possible at all to bind *strongly*  $\bar{K}$  mesons in nuclei and are such bound states sufficiently narrow to allow observation and identification? The current experimental and theoretical interest in this question was triggered back in 1999 by the suggestion of Kishimoto<sup>13</sup> to look for such states in the nuclear reaction  $(K^-, p)$  in flight, and by Akaishi and Yamazaki<sup>14</sup> who suggested to look for a  $\bar{K}NNN$   $I = 0$  state bound by over 100 MeV for which the main  $\bar{K}N \rightarrow \pi\Sigma$  decay channel would be kinemati-

cally closed. Some experimental evidence has been presented recently for candidate states in  $(K_{\text{stop}}^-, n)$  and  $(K_{\text{stop}}^-, p)$  reactions on  $^4\text{He}$  (KEK-PS E471,<sup>15,16</sup> respectively), in the  $(K^-, n)$  in-flight reaction on  $^{16}\text{O}$  (BNL-AGS, parasite E930<sup>17</sup>), and in  $K_{\text{stop}}^-$  reactions in Li and  $^{12}\text{C}$ , observing back-to-back  $\Lambda p$  pairs from  $K^- pp \rightarrow \Lambda p$  (DAΦNE-FINUDA<sup>18</sup>). None of it is sufficiently conclusive.

It is interesting then to study theoretically  $\bar{K}$  nuclear states in the range of binding energy  $B_{\bar{K}} \sim 100 - 200$  MeV, as suggested by these recent experiments, and in particular the width anticipated for such deeply bound states. The relatively shallow  $\bar{K}$ -nucleus potentials<sup>8,9</sup> derived from the microscopic construction by Ramos and Oset<sup>7</sup>, which are discussed in Section 2, are of no use in this context, since they cannot generate even within a dynamical calculation binding energies substantially greater than the potential depth of about 50 MeV. One must therefore depart from the microscopic approach in favor of a more phenomenologically inclined model which is constrained by data other than two-body  $\bar{K}N$  observables. The theoretical framework described here in Section 4, due to Mareš, Friedman and Gal<sup>5,19</sup>, is the relativistic mean field (RMF) model for a system of nucleons and one  $\bar{K}$  meson interacting through the exchange of scalar ( $\sigma$ ) and vector ( $\vec{\omega}, \vec{\rho}$ ) boson fields which are treated in the mean-field approximation. The RMF is a systematic approach used across the periodic table beyond the very light elements explored by other techniques, and it can be used also to study multi- $\bar{K}$  configurations and to explore the  $\bar{K}$  condensation limit<sup>20,21</sup>. Similar RMF calculations have been recently reported by the Frankfurt group for  $\bar{N}$  states in nuclei<sup>22,23</sup>.

## 2. $\bar{K}$ -nucleus potential from chirally motivated models

The Born approximation for the  $\bar{K}$ -nucleus potential due to the leading-order Tomozawa-Weinberg (TW) vector term of the chiral effective Lagrangian<sup>24</sup>,

$$V_{\bar{K}} = - \frac{3}{8f_{\pi}^2} \rho \quad (1)$$

where  $f_{\pi} \sim 93$  MeV is the pseudoscalar meson decay constant, yields sizable attraction  $V_{\bar{K}}(\rho_0) \sim -55$  MeV for  $\rho_0 = 0.16 \text{ fm}^{-3}$ . Iterating the TW term plus next-to-leading-order terms, within an *in-medium* coupled-channel approach constrained by the  $\bar{K}N - \pi\Sigma - \pi\Lambda$  data near the  $\bar{K}N$  threshold, roughly doubles this  $\bar{K}$ -nucleus attraction. It is found in these calculations (e.g. Ref.<sup>25</sup>) that the  $\Lambda(1405)$  quickly dissolves in the nuclear medium at finite densities, well below  $\rho_0$ , so that the repulsive free-space scattering length  $a_{K-p}$  becomes *attractive*, and together with the weakly density dependent attractive  $a_{K-n}$  it yields an attractive density dependent effective isoscalar scattering length  $a_{\text{eff}}(\rho)$ , denoted here also as  $b_0(\rho)$  (positive for attraction):

$$b_0(\rho) = \frac{1}{2}(a_{K-p}(\rho) + a_{K-n}(\rho)) , \quad b_0(\rho_0) \sim 0.9 \text{ fm} , \quad (2)$$

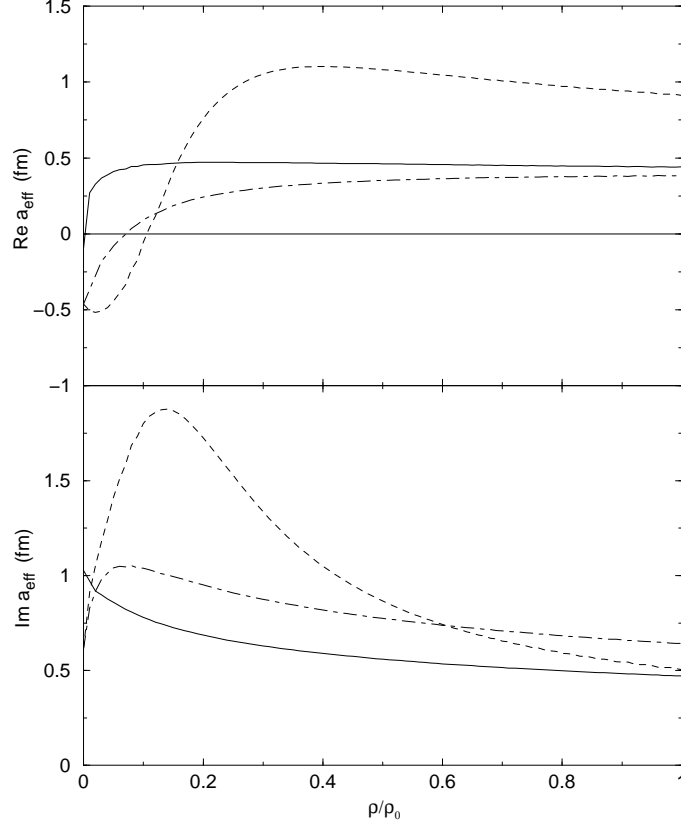


Fig. 2.  $\text{Re } a_{\text{eff}}$  (top) and  $\text{Im } a_{\text{eff}}$  (bottom) for the  $\bar{K}N$  scattering length as function of the density, calculated without requiring self consistency (dashed) and requiring it (dot-dash and solid).

leading to a strongly attractive  $\bar{K}$ -nucleus optical potential:

$$V_{\bar{K}}(r) = -\frac{2\pi}{\mu_{KN}} b_0(\rho) \rho(r), \quad \text{Re } V_{\bar{K}}(\rho_0) \sim -110 \text{ MeV}. \quad (3)$$

Here  $\mu_{KN}$  is the  $\bar{K}N$  reduced mass. However, when  $V_{\bar{K}}$  is calculated *self consistently* (SC), namely by including  $V_{\bar{K}}$  in the in-medium propagator used in the Lippmann-Schwinger equation determining  $V_{\bar{K}}$  as a  $\bar{K}$ -nucleus T matrix, the resultant  $\bar{K}$ -nucleus potential is only moderately attractive, with depth between 40 – 60 MeV. This is shown in Fig. 2, where the reduction of  $\text{Re } a_{\text{eff}}$  from the (non SC) dashed line to the (SC) solid line is clearly seen<sup>9</sup>. The reason for this weakening of the T matrix, approximately back to its TW potential kernel Eq. (1), is the strong absorptive effect of  $V_{\bar{K}}$  in the  $\bar{K}$ -nucleus propagator which suppresses the higher-order TW potential. It is the main reason that different theoretical calculations that obtain  $\bar{K}$ -nucleus potential depths  $\sim 100$  MeV without requiring SC, find

ultimately upon requiring SC depths  $\sim 50 \pm 10$  MeV at  $\rho_0$ <sup>6,7,9</sup>. The Akaishi and Yamazaki scheme of calculation<sup>14</sup> differs in many respects from the theoretical derivations here outlined. It gets rid of the  $\pi\Sigma$  coupled-channel effects too early in the calculation, essentially using a one-channel  $\bar{K}N$  energy-independent complex potential that fits the  $I = 0, 1$  scattering lengths and the position of the  $\Lambda(1405)$  unstable bound state for  $I = 0$ . This kind of construction is far from being unique, certainly with respect to models that use a comprehensive set of  $\bar{K}N$  low-energy data<sup>7,9</sup>. Furthermore, their analog of the TW potential kernel is considerably more attractive; and moreover, they do not impose the SC requirement, and it appears that the absorptive effect mentioned above is missing in their scheme. Therefore, their calculations have little common with the other ‘theoretical’ calculations in this field.

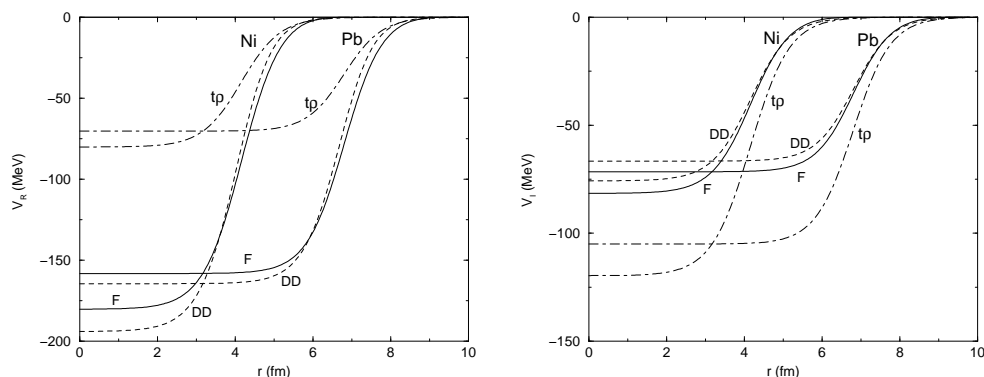


Fig. 3. Real part (left) and imaginary part (right) of the  $\bar{K}$ -nucleus potential for  $^{58}\text{Ni}$  and  $^{208}\text{Pb}$ , obtained in a global fit to  $K^-$ -atom data, for a  $tp$  potential, for the DD potential<sup>1</sup> and for potential F<sup>5</sup>, see text.

### 3. $\bar{K}$ -nucleus potential from fits to $K^-$ -atom data

The  $K^-$ -atom data used in global fits<sup>1</sup> span a range of nuclei from  $^7\text{Li}$  to  $^{238}\text{U}$ , with 65 level-shift and -width data points. Figure 3 shows the real part and the imaginary part of the  $\bar{K}$ -nucleus potential for  $^{58}\text{Ni}$  and  $^{208}\text{Pb}$  for a  $tp$  potential, where the complex strength  $t$  is fitted to these data, and for two density-dependent potentials marked by DD and F, also fitted to the same data. For the real part, the depth of the  $tp$  potential for a typical medium-weight to heavy nucleus is about 80 MeV, whereas the density-dependent potentials are considerably deeper, 150 – 200 MeV. These latter potentials also yield substantially lower  $\chi^2$  values of 103 and 84, respectively, than the value 129 for the  $tp$  potential. In particular, the shape of potential F departs appreciably from  $\rho(r)$  for  $\rho(r)/\rho_0 \lesssim 0.2$ , where the physics of the  $\Lambda(1405)$

6 *Avraham Gal*

still plays a major role. We note that, although the two density-dependent potentials have very different parameterizations, the resulting potentials are quite similar. In model F, considered in Ref. <sup>5</sup>, one divides configuration space into an ‘internal’ region and an ‘external’ region for both  $\text{Re } V_{\bar{K}}$  and  $\text{Im } V_{\bar{K}}$ :

$$b_0 \rightarrow B_0 F(r) + b_0 [1 - F(r)] , \quad (4)$$

using the function

$$F(r) = \frac{1}{e^x + 1} , \quad x = (r - R_x)/a_x , \quad R_x = R_{x0} A^{1/3} + \delta_x . \quad (5)$$

Here the parameter  $b_0$  represents the interaction in the external region, and may be held fixed at its free  $\bar{K}N$  value, whereas the parameter  $B_0$  represents the interaction inside the nucleus. The  $K^-$  atomic fit F used a fixed value  $a_x = 0.4$  fm, with little sensitivity for the precise value in the range  $0.2 - 0.5$  fm, optimizing for  $R_{x0} = 1.30 \pm 0.05$  fm,  $\delta_x = 0.8 \pm 0.3$  fm, thus implying that the modification of the free  $\bar{K}N$  interaction, namely the transition from the  $b_0$  term to the  $B_0$  term in Eq. (4), takes place at radii somewhat outside of the nuclear ‘half-density’ radius. Consequently,  $V_{\bar{K}}$  departs in shape from  $\rho(r)$  for densities less than about 20% of the central density.

## 4. $\bar{K}$ -nucleus RMF Dynamical Calculations

### 4.1. $\bar{K}$ -nucleus RMF methodology

In this model, expanded in Ref. <sup>5</sup>, the (anti)kaon interaction with the nuclear medium is incorporated by adding to  $\mathcal{L}_N$  the Lagrangian density  $\mathcal{L}_K$  <sup>20,21</sup>:

$$\mathcal{L}_K = \mathcal{D}_\mu^* \bar{K} \mathcal{D}^\mu K - m_K^2 \bar{K} K - g_{\sigma K} m_K \sigma \bar{K} K . \quad (6)$$

The covariant derivative  $\mathcal{D}_\mu = \partial_\mu + ig_{\omega K} \omega_\mu$  describes the coupling of the (anti)kaon to the vector meson  $\omega$ . The coupling of the (anti)kaon to the isovector  $\rho$  meson was neglected, a good approximation for the light  $N = Z$  nuclei. Whereas extending the nuclear Lagrangian  $\mathcal{L}_N$  by the Lagrangian  $\mathcal{L}_K$  does not affect the original form of the corresponding Dirac equation for nucleons, the presence of  $\bar{K}$  leads to additional source terms in the equations of motion for the meson fields  $\sigma$  and  $\omega_0$  to which the  $\bar{K}$  couples. The  $\bar{K}$  thus affects the scalar and vector potentials which enter the Dirac equation for nucleons, and this leads to a rearrangement or polarization of the nuclear core.

In order to preserve the connection to studies of  $K^-$  atoms, the Klein Gordon (KG) equation of motion for the  $\bar{K}$  is written in the form<sup>9</sup>:

$$[\Delta - 2\mu(B^{\text{s.p.}} + V_{\bar{K}} + V_c) + (V_c + B^{\text{s.p.}})^2] \bar{K} = 0 \quad (\hbar = c = 1), \quad (7)$$

where  $V_c$  is the  $K^-$  static Coulomb potential and  $\mu$  is the  $\bar{K}$ -nucleus reduced mass. The superscript s.p. in  $B^{\text{s.p.}} = B_{\bar{K}}^{\text{s.p.}} + i\Gamma_{\bar{K}}/2$  stands for the single-particle  $\bar{K}$  binding energy which is equal to the  $\bar{K}$  separation energy only in the static calculation. The

difference  $B_{\bar{K}}^{\text{s.p.}} - B_{\bar{K}}$  provides a measure of the nuclear rearrangement energy. The real part of the  $\bar{K}$  optical potential  $V_{\bar{K}}$  is then given by

$$\text{Re } V_{\bar{K}} = \frac{m_K}{\mu} \left[ \frac{1}{2} S - \left( 1 - \frac{B_{\bar{K}}^{\text{s.p.}} + V_c}{m_K} \right) V - \frac{V^2}{2m_K} \right], \quad (8)$$

where  $S = g_{\sigma K} \sigma$  and  $V = g_{\omega K} \omega_0$  are scalar and vector potentials due to the  $\sigma$  and  $\omega$  mean fields, respectively. Whereas  $\text{Re } V_{\bar{K}}$  is implicitly *state dependent* through the dynamical density dependence of the mean-field potentials  $S$  and  $V$ , as expected from a RMF calculation, it is here also explicitly state dependent through the  $[1 - (B_{\bar{K}}^{\text{s.p.}} + V_c)/m_K]$  energy-dependent factor multiplying the vector potential  $V$ .

Since the RMF approach does not address the imaginary part of the potential,  $\text{Im } V_{\text{opt}}$  was taken in a phenomenological  $t\rho$  form, where its depth was fitted to the  $K^-$  atomic data<sup>4</sup> with  $\text{Im } b_0 = 0.62$  fm. Note that the density  $\rho$  in the present calculations is no longer a static nuclear density, but is a *dynamical* entity affected by the  $\bar{K}$  interacting with the nucleons via boson fields. Suppression factors multiplying  $\text{Im } V_{\text{opt}}$  were introduced from phase-space considerations, taking into account the binding energy of the antikaon for the initial decaying state, and assuming two-body final-state kinematics for the decay products in the  $\bar{K}N \rightarrow \pi Y$  mesonic modes as well as in the  $\bar{K}N \rightarrow YN$  nonmesonic modes.

The coupled system of equations for nucleons and for the electromagnetic vector field  $A_0$ , for the  $\rho$  meson mean field, and for the mean fields  $\sigma$  and  $\omega_0$  with terms explicitly due to  $\bar{K}$  coupling, as well as the KG equation (7) for  $K^-$ , were solved self-consistently using an iterative procedure. In order to produce different values of binding energies,  $g_{\sigma K}$  was scaled down successively from its initial value  $g_{\sigma K}^{\text{atom}}$  appropriate to the  $K^-$ -atom fit and, once it reached zero,  $g_{\omega K}$  too was scaled down until the  $K^-$  1s state became unbound. Obviously, the good *global* fit to the atomic data is thus lost. Furthermore, in order to scan the region of large values of  $B_{K^-}$ , of order 200 MeV, we also scaled up  $g_{\sigma K}$  from its initial value, while keeping  $g_{\omega K}$  fixed at  $g_{\omega K}^{\text{atom}}$ . To give rough idea, whereas the static calculation gave  $B_{K^-} = 132$  MeV for the  $K^-$  1s state in  $^{12}\text{C}$ , using  $g_{\omega K}^{\text{atom}}, g_{\sigma K}^{\text{atom}}$ , the dynamical calculation gave  $B_{K^-} = 172$  MeV for this same state.

#### 4.2. Results for binding energies and widths

A comparison between the statically calculated (dashed lines) and the dynamically calculated (solid lines)  $B_{K^-}$  and  $\Gamma_{K^-}$  for the 1s state in  $^{12}\text{C}$  is shown in Fig. 4 as a function of the coupling-constant strenghts. We note that the width calculated dynamically for the 1s nuclear state in  $^{12}\text{C}$  does not fall below 50 MeV for the range of variation shown, whereas the corresponding limiting value of the statically calculated width is about 35 MeV. Another feature shown in Fig. 4 concerns the effect of the imaginary potential on the binding energy: the dynamically calculated binding energy  $B_{K^-}$  when  $\text{Im } V_{\bar{K}}$  is switched off is shown by the dotted line. It is clear that the absorptive potential  $\text{Im } V_{\bar{K}}$  acts *repulsively* and its inclusion leads to

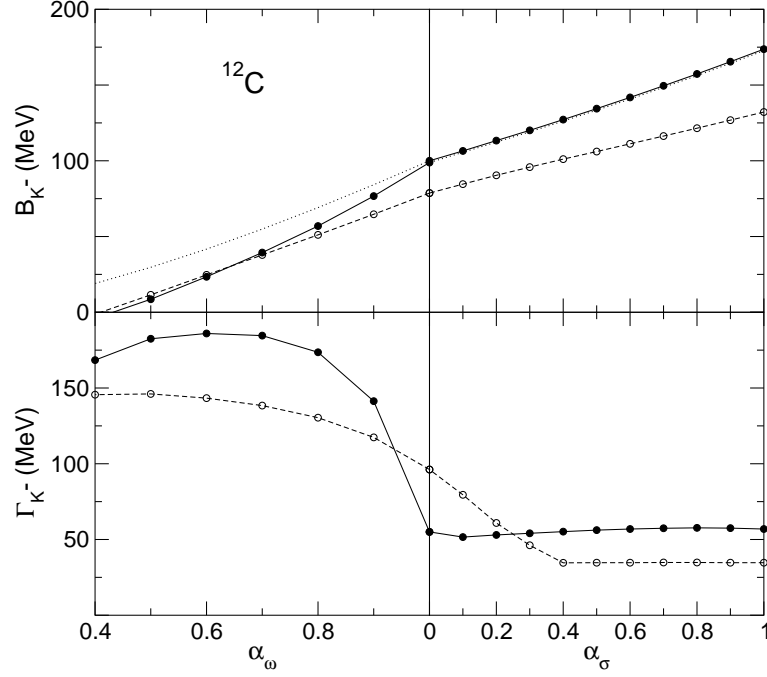


Fig. 4.  $1s$   $K^-$  binding energy and width in  $^{12}\text{C}$  calculated statically (dashed lines) and dynamically (solid lines) for the nonlinear RMF model NL-SH<sup>26</sup> as function of  $\alpha_\omega = g_{\omega K}/g_{\omega K}^{\text{atom}}$  and  $\alpha_\sigma = g_{\sigma K}/g_{\sigma K}^{\text{atom}}$ :  $\alpha_\omega$  is varied in the left panels as indicated, with  $\alpha_\sigma = 0$ , and  $\alpha_\sigma$  is varied in the right panels as indicated, with  $\alpha_\omega = 1$ . The dotted line shows the calculated binding energy when the absorptive  $K^-$  potential is switched off in the dynamical calculation.

less binding, particularly at low binding energies. The repulsive effect of  $\text{Im } V_{\bar{K}}$  gets weaker with  $B_{K^-}$ , along with the action of the kinematical phase-space suppression factors, and beginning with  $B_{K^-} \sim 100$  MeV it hardly matters for the calculation of  $B_{K^-}$  whether or not  $\text{Im } V_{\bar{K}}$  is included. The  $A$  dependence of these features is considered in Ref. <sup>5</sup>, leading to the following conclusions beginning approximately with  $^{12}\text{C}$ :

- The  $\bar{K}$  binding energy saturates, except for a small increase due to the Coulomb energy.
- The difference between the binding energies calculated dynamically and statically,  $B_{\bar{K}}^{\text{dyn}} - B_{\bar{K}}^{\text{stat}}$ , is substantial in light nuclei, increasing with  $B_{\bar{K}}$  for a given value of  $A$ , and decreasing monotonically with  $A$  for a given value of  $B_{\bar{K}}$ . It may be neglected only for very heavy nuclei. The same holds for the nuclear rearrangement energy  $B_{\bar{K}}^{\text{s.p.}} - B_{\bar{K}}$  which is a fraction of  $B_{\bar{K}}^{\text{dyn}} - B_{\bar{K}}^{\text{stat}}$ .
- The width  $\Gamma(B_{\bar{K}})$  decreases monotonically with  $A$ , as shown in Fig. 5.



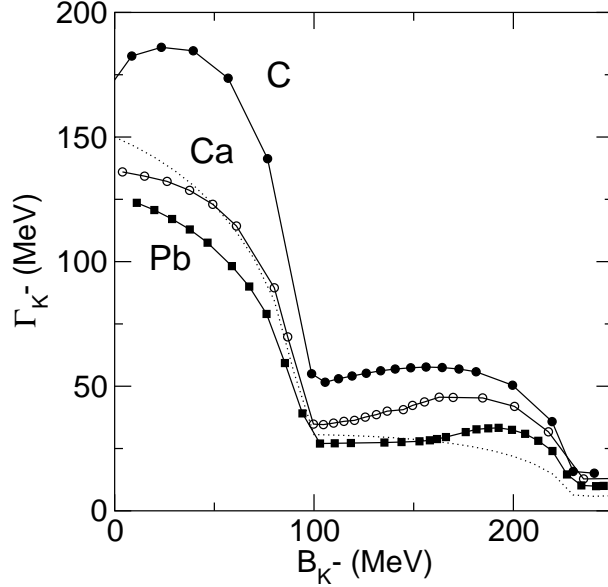


Fig. 5. Dynamically calculated widths of the  $1s$   $K^-$ -nuclear state in  $^{12}_K\text{C}$ ,  $^{40}_K\text{Ca}$  and  $^{208}_K\text{Pb}$  as function of the  $K^-$  binding energy for nonlinear RMF models. The dotted line is for a static nuclear-matter calculation with  $\rho_0 = 0.16 \text{ fm}^{-3}$ .

Figure 5 shows calculated widths  $\Gamma_{K^-}$  as function of the binding energy  $B_{K^-}$  for  $1s$  states in  $^{12}_K\text{C}$  and  $^{40}_K\text{Ca}$ , using the nonlinear NL-SH version<sup>26</sup> of the RMF model, and in  $^{208}_K\text{Pb}$  using the NL-TM1 version<sup>27</sup>. The dotted line shows the static ‘nuclear-matter’ limit

$$\Gamma_{K^-} = \frac{f}{1 - \frac{B_{K^-}}{m_K}} \Gamma_{K^-}^{(0)}, \quad (9)$$

where  $f$  is the phase-space suppression factor used in the dynamical calculations, and  $\Gamma_{K^-}^{(0)}$  is given by

$$\Gamma_{K^-}^{(0)} = \frac{4\pi}{\mu_{KN}} \text{Im } b_0 \rho_0, \quad (10)$$

for the static value  $\text{Im } b_0 = 0.62 \text{ fm}$  used in the calculations and for  $\rho_0 = 0.16 \text{ fm}^{-3}$ . Eq. (10) holds for a  $K^-$  Schrodinger wavefunction which is completely localized within the nuclear central-density  $\rho_0$  region. The additional factor  $(1 - B_{K^-}/m_K)^{-1}$  in Eq. (9) follows from using the KG equation rather than the Schrodinger equation. It is clearly seen that the dependence of the width of the  $K^-$  nuclear state on its binding energy follows the shape of the dotted line for the static nuclear-matter limit of  $\Gamma_{K^-}$ , Eq. (9). This dependence is due primarily to the binding-energy dependence of the suppression factor  $f$  which falls off rapidly until  $B_{K^-} \sim 100 \text{ MeV}$ , where the dominant  $\bar{K}N \rightarrow \pi\Sigma$  gets switched off, and then

stays rather flat in the range  $B_{K^-} \sim 100 - 200$  MeV where the width is dominated by the two-nucleon absorption modes. The larger values of width for the lighter nuclei are due to the dynamical nature of the RMF calculation, whereby the nuclear density is increased by the polarization effect of the  $K^-$ . The widths calculated in the range  $B_{K^-} \sim 100 - 200$  MeV assume considerably larger values than what the static calculation of the dotted line shows (except for Pb in the range  $B_{K^-} \sim 100 - 150$  MeV). Adding perturbatively the residual width neglected in this calculation, mainly due to the  $\bar{K}N \rightarrow \pi\Lambda$  secondary mesonic decay channel, a representative value for a lower limit  $\Gamma_{\bar{K}} \sim 50 \pm 10$  MeV holds in the binding energy range  $B_{K^-} \sim 100 - 200$  MeV.

#### 4.3. Nuclear polarization effects

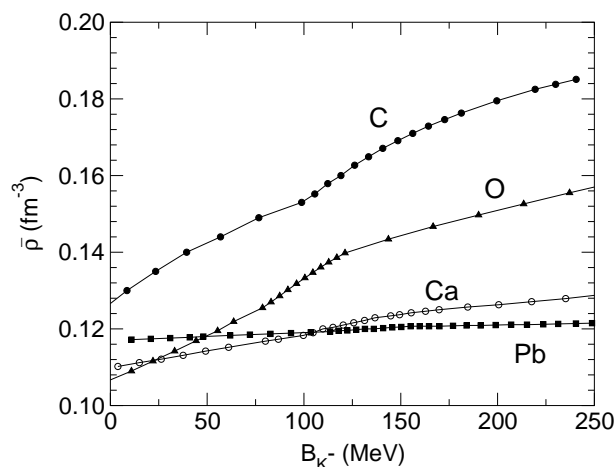


Fig. 6. Calculated average nuclear density  $\bar{\rho}$  for  ${}_{K^-}^{12}\text{C}$ ,  ${}_{K^-}^{16}\text{O}$ ,  ${}_{K^-}^{40}\text{Ca}$  and  ${}_{K^-}^{208}\text{Pb}$  as function of the  $1s$   $K^-$  binding energy for the NL-SH RMF model <sup>26</sup>.

Figure 6 shows the calculated average nuclear density  $\bar{\rho} = \frac{1}{A} \int \rho^2 d\mathbf{r}$  as a function of  $B_{K^-}$  for the same  $K^-$  nuclear  $1s$  states as in Fig. 5 and for  $1s$  states in  ${}_{K^-}^{16}\text{O}$ . The average nuclear density  $\bar{\rho}$  increases substantially in the light  $K^-$  nuclei, for the binding-energy range shown here, to values about 50% higher than for these nuclei in the absence of the  $K^-$  meson. The increase of the central nuclear densities is even bigger, as demonstrated in the next figure, but is confined to a small region of order 1 fm from the origin.

Figure 7 shows on the left-hand side calculated nuclear densities of  ${}_{K^-}^{12}\text{C}$  for several values of the  $1s$   $K^-$  binding energies. The purely nuclear density, in absence of the  $K^-$  meson, is given by the dashed curve. The maximal value of the nuclear density is increased by up to 75% in the range of binding energies spanned in the

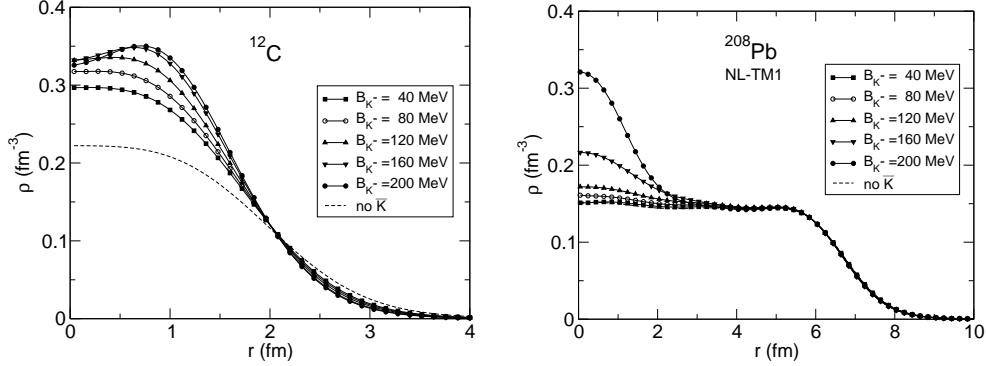


Fig. 7. Calculated nuclear density  $\rho$  of  $^{12}\text{C}$  (left) and of  $^{208}\text{Pb}$  (right) for several  $B_{K^-}$  values of  $1s$   $K^-$  nuclear states, using the nonlinear RMF models NL-SH<sup>26</sup> and NL-TM1<sup>27</sup>, respectively.

figure, and the enhancement is close to uniform over the central region of  $r \lesssim 1$  fm, decreasing gradually to zero by  $r = 2$  fm which already marks the nuclear surface. In this fairly small nucleus, the density is enhanced over a substantial portion of the nucleus. This is different than in heavier nuclei, as shown on the right-hand side of Fig. 7 for  $^{208}\text{Pb}$ . Here, the enhancement of the maximal density (at the center of the nucleus) is appreciable only for  $B_{K^-}$  values above 150 MeV, reaching a factor of two, but it subsides almost completely by  $r = 2$  fm which is still well within the nuclear volume. As a result, the *average* nuclear density of  $^{208}\text{Pb}$  shown in Fig. 6 is only weakly enhanced as function of  $B_{K^-}$ .

The upper and lower panels of Fig. 8 show the calculated nuclear rms radius and the  $1s$  and  $1p$  neutron single-particle energies  $E_n$ , respectively, for  $^{16}\text{O}$  as a function of  $B_{K^-}$ . It is clear that the polarization effect of the  $1s$   $K^-$  bound state on the  $1s$  nuclear core is particularly strong. The differences between the linear and nonlinear models reflect the different nuclear compressibility and the somewhat different nuclear sizes obtained in the two models. The increase in the nuclear rms radius of  $^{16}\text{O}$  for large values of  $B_{K^-}$  is the result of the reduced binding energy of the  $1p_{1/2}$  state, due to the increased spin-orbit term.

## 5. Conclusions

In this talk I reviewed the phenomenological and theoretical evidence for a substantially attractive  $\bar{K}$ -nucleus interaction potential, from a ‘shallow’ potential of depth 40 – 60 MeV to a ‘deep’ potential of depth 150 – 200 MeV at  $\rho_0$ . I then reported on recent *dynamical* calculations<sup>5</sup> of deeply bound  $K^-$  nuclear states across the periodic table, aimed at providing lower limits on the widths expected for binding energies in the range of 100 – 200 MeV. Substantial polarization of the core nucleus was found in light nuclei. Almost universal dependence of  $\bar{K}$  widths on the binding energy was found, for a given nucleus, reflecting the phase-space suppression factor

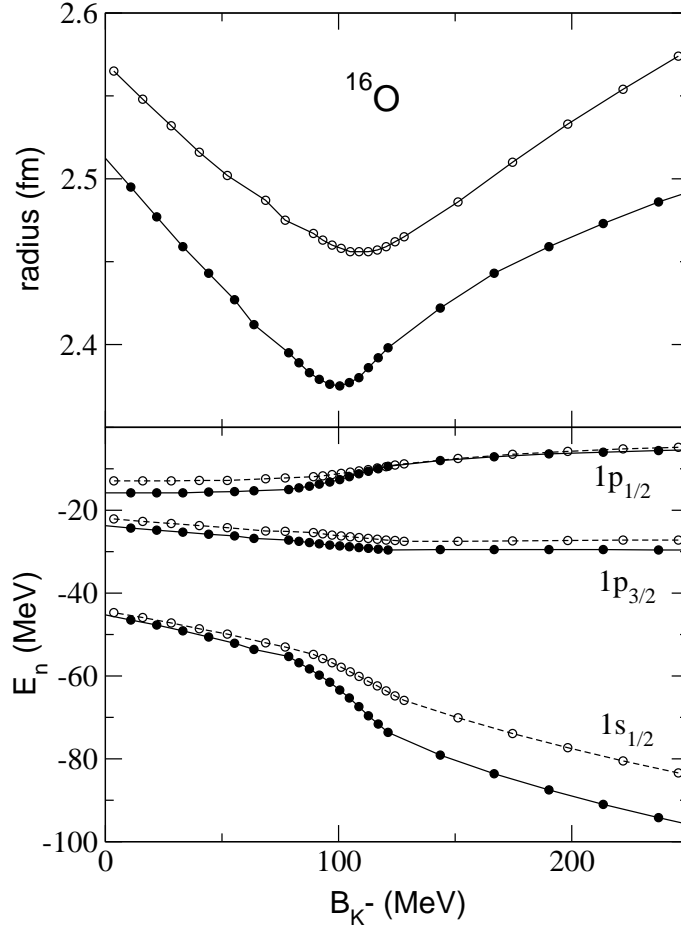


Fig. 8. Nuclear rms radius and neutron single-particle energies for  ${}_{K^-}^{16}\text{O}$  as function of the  $1s$   $K^-$  binding energy, for the linear RMF model L-HS <sup>28</sup> (open circles) and the nonlinear RMF model NL-SH <sup>26</sup> (solid circles).

on top of the increase provided by the density of the compressed nuclear cores. The present results already provide useful guidance for the interpretation of recent experimental results by placing a lower limit  $\Gamma_{\bar{K}} \sim 50 \pm 10$  MeV. For lighter nuclear targets such as  ${}^4\text{He}$ , where the RMF approach becomes unreliable but where nuclear polarization effects are found larger using few-body calculational methods<sup>14,29</sup>, one anticipates larger widths for  $\bar{K}$  deeply bound states, if such states do exist.

### Acknowledgements

I wish to thank my collaborators Eli Friedman and Jiří Mareš for stimulating discussions, and Horst Stöcker for supporting my participation in ISHIP 2006 through

funds allocated by the Alexander von Humboldt Foundation. This work was supported in part by the Israel Science Foundation, Jerusalem, grant 757/05.

## References

1. C.J. Batty, E. Friedman, A. Gal, Phys. Rep. **287** (1997) 385.
2. E. Friedman, A. Gal, C.J. Batty, Phys. Lett. **B308** (1993) 6.
3. E. Friedman, A. Gal, C.J. Batty, Nucl. Phys. **A579** (1994) 518.
4. E. Friedman, A. Gal, J. Mareš, A. Cieplý, Phys. Rev. **C60** (1999) 024314.
5. J. Mareš, E. Friedman, A. Gal, Nucl. Phys. **A770** (2006) 84.
6. J. Schaffner-Bielich, V. Koch, M. Effenberger, Nucl. Phys. **A669** (2000) 153.
7. A. Ramos, E. Oset, Nucl. Phys. **A671** (2000) 481.
8. A. Baca, C. García-Recio, J. Nieves, Nucl. Phys. **A673** (2000) 335.
9. A. Cieplý, E. Friedman, A. Gal, J. Mareš, Nucl. Phys. **A696** (2001) 173.
10. E. Friedman, A. Gal, Phys. Lett. **B459** (1999) 43.
11. E. Friedman, A. Gal, Nucl. Phys. **A658** (1999) 345.
12. E. Friedman, A. Gal, in *Frascati Physics Series Vol. XVI, Proc. III Int. Workshop on Physics and Detectors for DAΦNE*, eds. S. Bianconi *et al.* (LNF, Frascati, 1999), p. 677.
13. T. Kishimoto, Phys. Rev. Lett. **83** (1999) 4701.
14. Y. Akaishi, T. Yamazaki, in *Frascati Physics Series Vol. XVI, Proc. III Int. Workshop on Physics and Detectors for DAΦNE*, eds. S. Bianconi *et al.* (LNF, Frascati, 1999), p. 59; Phys. Rev. **C65** (2002) 044005.
15. M. Iwasaki, *et al.*, nucl-ex/0310018; T. Suzuki, *et al.*, Nucl. Phys. **A754** (2005) 375c.
16. T. Suzuki, *et al.*, Phys. Lett. **B597** (2004) 263.
17. T. Kishimoto, *et al.*, Nucl. Phys. **A754** (2005) 383c.
18. M. Agnello, *et al.*, Phys. Rev. Lett. **94** (2005) 212303.
19. J. Mareš, E. Friedman, A. Gal, Phys. Lett. **B606** (2005) 295.
20. J. Schaffner, A. Gal, I.N. Mishustin, H. Stöcker, W. Greiner, Phys. Lett. **B334** (1994) 268.
21. J. Schaffner, I.N. Mishustin, Phys. Rev. **C53** (1996) 1416.
22. T. Bürvenich, I.N. Mishustin, L.M. Satarov, J.A. Maruhn, H. Stöcker, W. Greiner, Phys. Lett. **B542** (2002) 261.
23. I.N. Mishustin, L.M. Satarov, T.J. Bürvenich, H. Stöcker, W. Greiner, Phys. Rev. **C71** (2005) 035201.
24. T. Waas, M. Rho, W. Weise, Nucl. Phys. **A617** (1997) 449; and references therein.
25. T. Waas, N. Kaiser, W. Weise, Phys. Lett. **B379** (1996) 34.
26. M.M. Sharma, M.A. Nagarajan, P. Ring, Phys. Lett. **B312** (1993) 377.
27. Y. Sugahara, H. Toki, Nucl. Phys. **A579** (1994) 557.
28. C.J. Horowitz, B.D. Serot, Nucl. Phys. **A368** (1981) 503.
29. A. Doté, H. Horiuchi, Y. Akaishi, T. Yamazaki, Phys. Lett. **B590** (2004) 51; Phys. Rev. **C70** (2004) 044313.